Numerical simulations of turbulent flow in an electromagnetically levitated metallic droplet using k-Ω SST and Reynolds stress models

Olga Budenkova, Yves Delannoy, Annie Gagnoud

Submitted to Magnetohydrodynamics after revision.
Be aware of some modifications in the final text

Numerical simulations of turbulent flow in the electromagnetically levitated metallic droplet using $k-\omega$ SST and Reynolds Stress models

O. Budenkova, A. Gagnoud, Y. Delannoy

Univ. Grenoble Alpes, CNRS, Grenoble INP, SIMAP, F-38000 Grenoble, France

Electromagnetic levitation of a metallic droplet in the microgravity conditions is modelled accounting for the droplet shape variation, its displacement and turbulent character of the flow in the system. Three different models are applied for description of turbulent flow in the droplet: $k-\omega$ SST model and two models based on Reynolds stresses (RSM), all of them resulted in a qualitatively similar flow inside a droplet. Use of RSM-based models leads to a sharper interface of a droplet in volume-of-fluid calculations compared to the $k-\omega$ SST model. Two RSM models predict value of the surface tension close to a theoretical one, yet, both fail in predicting of viscosity of the droplet's material.

Introduction In microgravity conditions, electromagnetic levitation (EML) is used both as an environment and a tool allowing measurements of thermophysical properties of liquid metals. At present, experimental procedures with EML are implemented in MSL-Lab at International Space Station and in TEMPUS facility used in parabolic flights [1]. At the beginning of experiment a solid metallic sample is placed at the center of an electromagnetic inductor (Fig. **??**) where it is retained near the equilibrium position by quadrupole AC magnetic field. The latter is created with use of alternate current $j_{ext,p}$ with frequency $f_p \approx 150$ kHz supplied to the inductor with a constant phase shift $\Delta\varphi_p = \pi$ between the upper and lower coils. Some amount of heat released in the sample due to circulation of eddy current serves for sample pre-heating. Further, the sample is heated, melted and over-heated by supplying to the inductor second alternate current $j_{ext,d}$ with frequency $f_d \approx 310$ kHz without any phase shift between coils that creates bipolar AC magnetic field. At required temperature of the sample supply of $j_{ext,d}$ current to the inductor is stopped and re-activated later in different modes for short periods of time during the cooling phase of the liquid sample to get various sets of data. Two high-speed video cameras film the sample from its lateral side and from the top and temperature of the sample is measured at different areas with pyrometers.

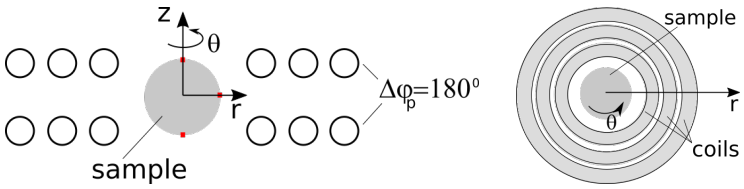

Figure 1: Scheme of the inductor used in microgravity conditions, lateral and top view. Positioning current $j_{ext,p}$ is supplied with phase difference $\Delta\varphi_p = \pi$ between the upper and the lower coils that creates quadruple magnetic field, bipolar magnetic field is created with the second current $j_{ext,d}$ without phase shift between coils

In particular, to measure surface tension and viscosity of liquid melt, the second (bipolar) AC magnetic field is briefly activated to "squeeze" slightly the droplet. When this field is switched off, the droplet gradually restores its spherical shape yet this happens through decaying oscillations between prolate and oblate spheroid whose eccentricity close to zero [2, 3, 4]. According to the Lamb's theory [5], surface tension at interface between liquid and surrounding media is related to the frequency of surface oscillation, denoted hereafter f_γ, while viscosity of the liquid is defined by decrement of oscillations' amplitude. This theory assumes only potential flow inside the droplet due to stretching and compression of the latter, however, AC magnetic field which retains droplet in space is always active and corresponding Lorentz force drives recirculating flow inside the droplet. Effect of the latter on measurement remains unclear despite efforts made to estimate it both for microgravity and terrestrial conditions [4, 6, 7, 8, 9].

Numerical simulation, which seems to be a unique approach to reveal effect of convection on behavior of the droplet's surface, meets difficulties for several reasons. Firstly, electromagnetic fields, hydrodynamic flow in the droplet and surrounding it media and shape and position of the droplet should be calculated in coupled manner. Second, in the course of measurement procedure, i.e. during simulations, character of the flow inside the droplet varies from nearly laminar to turbulent. The latter originates by rapid motion of droplet surface while recirculating flow driven by Lorentz force is characterized by low Reynolds number and could be supposed laminar. Thirdly, turbulent flow in the droplet belongs to those kinds of flows for which empirical parameters existing in each turbulent model are not really defined. One can suppose that choice of turbulent model can affect simulations results. Indeed, this was confirmed by numerical study of Berry et al. [7] where electromagnetic levitation of the droplet in microgravity was modeled using laminar, $k-\varepsilon$ and RNG models for turbulence and Volume-Of-Fluid method (VOF) was used to account for shape variation of the droplet. Similar conclusion was made by Spitans et al. [8] where $k-\varepsilon$, $k-\omega$ SST and LES turbulent models were studied for modeling of a droplet levitation with the presence of the gravity force. In both works [7, 8] electromagnetic force calculated with a different software was introduced into momentum equations as a source terms after its interpolation from one grid used for electromagnetic modeling to another grid for hydrodynamic calculations used in ANSYS FLUENT. Data exchange between programs solving electromagnetic problem and hydrodynamic one coupled with shape calculations was made either at each time step or once per several time steps. Both studies provided good agreement with theory regarding prediction of the surface tension recalculated from the frequency of droplet's oscillation. Yet, a classical relation between viscosity of the droplet and decrement of the oscillations [5] was not confirmed for viscosity proper to liquid metals.

Present work continues this series of numerical study of electromagnetic levitation of a droplet and uses Reynolds Stress models for turbulent flow which were not considered in previous simulations. ANSYS Fluent is used to obtain non-stationary solution of hydrodynamic equations coupled with calculations of shape of the droplet due to use of VOF model. Electromagnetic problem is solved with home-made module based on user-defined functions and implemented into ANSYS Fluent as an add-on library [9, 10]. Use of only one software allows us to make modeling with unique calculation grid, i.e. to avoid problems of data interpolation. Unsteady modeling is performed using iterative segregated approach and update of distribution of electromagnetic forces required for hydrodynamic equations and distribution of electrical conductivity required by electromagnetic equations is done at each iteration within a time step.

1. Problem description The problem is considered axially symmetric and a volume-of-fluid (VOF) approach was adopted to treat the droplet displacement and to model further the oscillation of its surface. In experiments inductor with sample are placed inside a sealed quartz chamber which is generally filled with argon to decrease oxidation and evaporation of the sample, that is taken into simulations.

1.1. Volume-of-fluid model The principle of the Volume-Of-Fluid (VOF) method is to use a single set of momentum and energy equations for all fluids in the system and to track a volume fraction α_i of each of fluids throughout the calculation domain in each mesh cell, providing that, for example, for two liquids

$$\alpha_1 + \alpha_2 = 1$$

Zone of transition of α_i from unity to zero corresponds to the interface between participating fluids. Surface tension is introduced into momentum equation as volume force $\mathbf{F}_\gamma$, and is given by Eq.1 if only two fluids exist in the system.

$$\mathbf{F}_\gamma = 2\gamma \frac{\alpha_1\rho_1 k_1 \nabla\alpha_2 + \alpha_2\rho_2 k_2 \nabla\alpha_1}{\rho_1 + \rho_2} \quad \text{with} \quad k_i = \nabla \cdot \frac{\nabla\alpha_i}{|\nabla\alpha_i|} \tag{1}$$

here γ is a surface tensions between two fluids, ρ_1 and ρ_2 are proper densities of each of fluids and k_i is a curvature of the interface. Lorentz forces obtained from solution of electromagnetic problem as explained below and given by Eq.7 are also introduced into momentum equations. Density and viscosity in hydrodynamic equations are calculated using linear mixture laws which for any physical property ψ with proper values ψ_1 and ψ_2 in each of two fluids is given as

$$\psi = \alpha_1\psi_1 + \alpha_2\psi_2 \tag{2}$$

This applies also to calculation of electric conductivity σ.

Whole calculation domain with the part where hydrodynamic simulations were made are shown in Fig. 2. Similar to experiment, the second fluid surrounding the sample is argon. Since treatment of conditions at the droplet interface is made with VOF approach, non-slip boundary conditions for hydrodynamic equations are required only at surface of inductor coils and at chamber walls. Simulations are performed for microgravity environment and temperature related effect are not considered. Turbulent models used in simulations are discussed in the subsection 1.3.

1.2. Electromagnetic calculations Modeling of electromagnetic phenomena is based on calculation of the components of magnetic vector potential $\mathbf{A}$ and scalar electric potential V related by following equations

$$\nabla^2\mathbf{A}_i = \mu_0\sigma\left(\nabla V_i + \frac{\partial\mathbf{A}_i}{\partial t}\right) \tag{3}$$

$$\nabla\cdot(\sigma\nabla V_i) = \nabla\cdot\left(\sigma\frac{\partial\mathbf{A}_i}{\partial t}\right) \tag{4}$$

$$\nabla\cdot\mathbf{A}_i = 0 \tag{5}$$

here index $i = p, d$ corresponds to the field created either by positioning current ($i = p$) or by heating current ($i = d$), $\mu_0 = 4\pi\cdot10^{-7}$ H/m is magnetic permeability of the free space, σ is electric conductivity of the media defined for the liquid

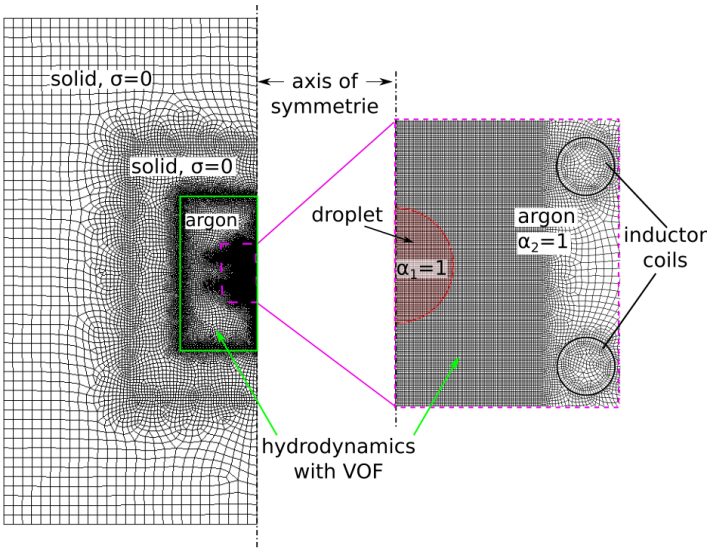

Figure 2: Scheme of the calculation domain in (r, z) meridional plane: whole domain with central chamber filled with argon (left) with zoom to the central part on the droplet and (right). Electromagnetic simulations are performed throughout the whole domain, hydrodynamic calculations are done inside domain marked with green color

zone via the mixture law given above by Eq. 2. Condition given by equation 5 corresponds to Coulomb gauge and is used implicitly in equations 3-4. External current is imposed in the coil of inductor as explained in appendix A. Further, magnetic inductions and density of electric current for each of field can be found from solutions obtained for $\mathbf{A}$ and V as

$$\mathbf{B}_i = \nabla \times \mathbf{A}_i \quad \text{and} \quad \mathbf{j}_i = \sigma \left(-\nabla V - \frac{\partial \mathbf{A}_i}{\partial t} \right) \tag{6}$$

Then Lorentz force due to interaction of eddy current and AC magnetic field inside the droplet is given as

$$\mathbf{F}_{L,i} = \mathbf{j}_i \times \mathbf{B}_i \tag{7}$$

Consequently, force $\mathbf{F}_{L,p}$ which exists due to circulation in the coil positioning AC current $\mathbf{j}_{ext,p}$ retains the droplet while force $\mathbf{F}_{L,d}$, which appears due to activation of heating current $\mathbf{j}_{ext,d}$, is used to deform the droplet, i.e. to trigger its oscillations.

Solution of electromagnetic problem is performed with complex harmonics that produces system of equations corresponding to initial one given by Eqs.3-4 but for real and complex part of all variables, details are presented in the Appendix. Then spatial discretization of obtained equations is formulated for finite volume method and is implemented into ANSYS FLUENT via User-Defined functions. It should be stresses that boundary conditions at the surface of the droplet are not required since the latter, in fact, does not exist in VOF approach but is presented as a thin spatial layer with variable properties. Conditions at the external boundary of the calculation domain shown in Fig. 2 are discussed in the Appendix A.

1.3. Turbulent models In simulations we tested $k - \omega$ SST model and two Reynolds Stress model (RSM). The first approach was chosen due to its ability to treat most of "canonic" flows while Reynolds stress models were chosen because

they are suitable for anisotropic flows. All these models are built on the assumption that velocity components and pressure of flow can be presented as a composition of their mean and fluctuating values: $\xi =< \xi > +\xi'$. The $k-\omega$ SST model uses the Boussinesque approximation which relates Reynolds stress tensor composed of mean values of products of the velocity's fluctuating components $R_{ij} =< u_i' u_j' >$ with gradients of the mean velocity via eddy viscosity (turbulent viscosity) η_t. This value is supposed to be isotropic and is related to the kinetic energy of the pulsating components k_t, and to specific dissipation of the latter per unit of time. Description of the turbulent flows using model $k-\omega$ SST results in two more differential equations for k_t and ω, which are solved simultaneously with continuity and momentum equations for the mean flow component. Equations for k_t and ω contain additional semi-empirical terms which ideally should be defined from experimental measurement and which are aimed to capture the specific character of the flow depending on the external conditions.

Reynolds Stress model does not use the Boussinesque approximation and differential equations required for calculation of components of R_{ij} tensor are solved along with Navier-Stokes equations whereas closure semi-empirical relations are used for higher correlation terms and for their derivatives. The difference between two RSM models used in simulations lies in treatment of a pressure-strain term $\phi_{ij} =< p(\partial u_i'/\partial x_j + \partial u_j'/\partial x_i) >$ which appears in equations for R_{ij}. One model, linear pressure-strain model, denoted hereafter as RSM-ε, relates ϕ_{ij} to turbulent energy k_t and to its dissipation ε. Another chosen model, low-Re Stress-Omega model, denoted hereafter RSM-ω, presents pressure-strain term ϕ_{ij} with turbulent energy k_t and its specific dissipation ω, similar to $k-\omega$ SST model. Two more options are proposed in ANSYS FLUENT for the treatment of the same term, but were not tested. For details the reader is proposed to refer to documentation [11].

2. Results Simulations were made for a liquid sample initially having a spherical shape with the radius $R_0 = 3.26$mm, same as in experiments. Values for surface tension, dynamic viscosity and density were taken equal to those measured in the experiment: $\gamma = 1.7$N/m, $\eta_{Ni} = 0.008$Pa·s, and $\rho_{Ni} = 8000$kg/m^3, respectively. This set of data corresponds to a Ni-based material for which electric conductivity can be taken $\sigma = 10^6$S/m. For the argon which fills the chamber the following values were taken for density and dynamic viscosity $\rho_{Ni} = 1.62$kg/m^3 and $\eta_{Ar} = 0.000021$Pa·s.

At initial state a spherical droplet is placed near the equilibrium position, i.e. with its centre at (r_0, z_0), in axial symmetry $r_0 = 0$. In terms of VOF approach this means that initial distribution of volume fractions α_1 corresponding to the droplet is:

$$\alpha_1(r,z) = \begin{cases} 1, & \text{if } (r-r_0)^2 + (z-z_0)^2 \le R_0^2 \\ 0, & \text{otherwise} \end{cases} \tag{8}$$

and rest of volume containing the inductor and the sample is filled with a gas. At $t > 0$ positioning current $\mathbf{j}_{ext,p}$ is activated in the inductor that leads to slight deformation of the droplet and its oscillations as a whole in the vertical direction. When the droplet is nearly stabilized, electric current $\mathbf{j}_{ext,d}$ to trigger its deformation is activated for a period of 0.1s, then this current is stopped and relaxation of the droplet back to its equilibrium shape is observed. The following expressions are adopted to estimate the maximal horizontal radius and vertical diameter of the droplet R_r and D_z during simulations:

$$R_r = max(r \cdot \alpha_1) \tag{9}$$

$$D_z = max(z \cdot \alpha_1) - min(z \cdot \alpha_1) \tag{10}$$

here r and z is radial and axial coordinate.

2.1. Results for the droplet before triggering its oscillations Instantaneous flow patterns inside the droplet obtained with $k-\omega$ SST model, RSM-ε and RSM-ω models once the droplet is almost stabilized consist of two pair of vortices: two smaller vortices are near droplet's equator and two others are near the poles (Fig. 3). The flow calculated with RSM-based models and presented for the same moment of time is almost identical but the shape of vortices is slightly different from that calculated with $k-\omega$ SST model. This can be probably assigned to small displacement of the droplet which persist in calculations with RSM models and $k-\omega$ SST model with slightly different amplitudes.

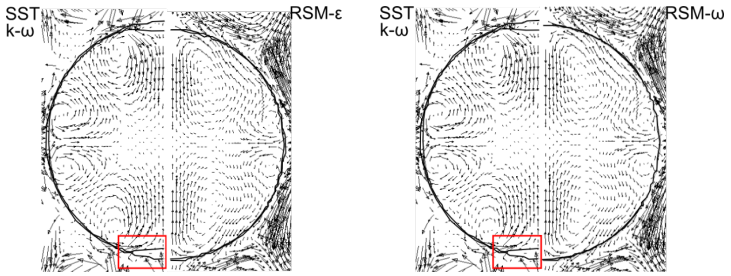

Figure 3: Instantaneous flow pattern inside the droplet obtained with $k-\omega$ SST model and RSM-ε (left), and $k-\omega$ SST model and RSM-ω (right), maximal velocity for all models is ≈ 2.3cm/s. Solid lines correspond to the value of droplet's phase fraction α_1=0.995 and α_1=0.98. Vectors outside the droplet show velocity in argon surrounding the droplet

Yet, another difference exists which has more importance for numerical studies. The contour of the droplet in Fig.2 is presented with two lines corresponding to and which almost coincide in simulations with both RSM models but diverge near droplet's poles in calculation with $k-\omega$ SST model. Actually, in simulations with the latter approach detachment of small fractions of the droplet at its poles was observed and could not be avoided with variations of numerical parameters like under-relaxation factors and Courant number.

Another difference between the $k-\omega$ SST model and RSM-based models can be found in the presentation of the turbulence inside the droplet (Fig.4).

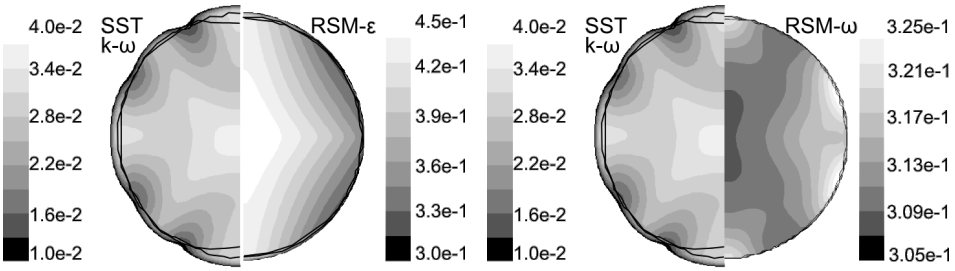

Figure 4: Instantaneous pattern for turbulent viscosity inside the droplet obtained with $k-\omega$ SST model and RSM-ε (left), and $k-\omega$ SST model and RSM-ω (right). Solid lines correspond to the value of droplet's phase fraction α_1=0.995 and α_1=0.98. Vectors outside the droplet show velocity in argon

It is obtained that the turbulent viscosity is ten times higher in the both RSM based models than in the $k-\omega$ SST. Surprisingly, in $k-\omega$ SST and RSM-ε models the maximal turbulent viscosity occurs near the axis of symmetry and minimal values at the surface, that means that there is more dissipation of the turbulent energy or its less production. Conversely, the RSM-ω model gives its minimal value at the axis and maximal at the surface.

2.2. Oscillations of the droplet's surface When axial translation motion of the droplet caused by initiating of the positioning electric current in the inductor becomes less intense, the second current in the coils is activated in simulations for 0.1s. During this period of time the droplet tends to take the form of prolate spheroid that is accompanied with oscillations of its surface (5). Introduced deformation of the droplet diameter is about 1mm that is about 15% with respect to its initial value. Once the second current is stopped, the droplet returns to a nearly spherical shape which is also accompanied with oscillations whose characteristics are measured in the experiment. In simulations performed with RSM-ε and RSM-ω models for turbulent flows results for variation of D_z in time (given by eq.10) appear slightly different .

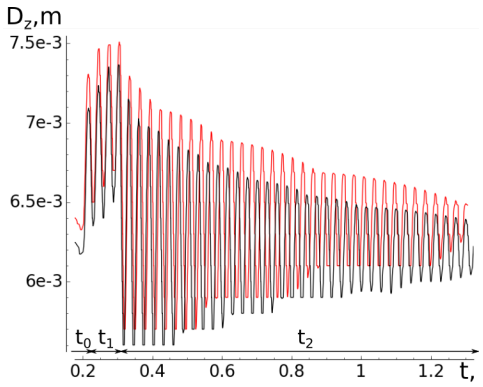

Figure 5: Variation of the vertical diameter of the droplet in simulations obtained with two turbulent models, black line is for RSM-ε model and red line for RSM-ω model. Indicated periods of time correspond to alimentation of the inductor with positioning current only (t_0 and t_2) and to activation of both currents $j_{ext,p}$ and $j_{ext,p}$ during the period t_1

In Fig.6 Fourier spectrum for oscillations of D_z is shown for two models of turbulence. With both models the frequency of the oscillations observed in simulations is close to the theoretical value of 35.7Hz: the RSM-ε models gives 35.1Hz, and the RSM-ω 34Hz. It is interesting to note that for both models some oscillations with a frequency nearly doubled (about 70Hz) seems to be captured by simulations that correspond to the second oscillation mode. It is probably an indication that the initial deformation of the droplet was too large and does not satisfy requirement of a small perturbation. It can be seen also that distribution of energy of oscillations of various frequencies is more uniform for lower range in case of use of RSM-ω that is probably related to a higher non-uniformity of turbulent viscosity observed in this case.

3. Conclusions The work presents numerical modeling of electromagnetic levitation of a metallic droplet, deformation of the latter using additional

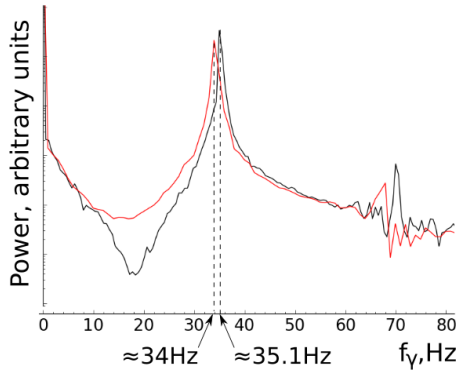

Figure 6: Fourier spectrum for oscillations of the value of vertical diameter of the droplet presented in Fig.5 and calculated with the use of RSM-ε model (black line) and RSM-ω model (red line) for the turbulent flow. Theoretical value for the frequency of oscillations is 35.7Hz

electromagnetic force and return of the droplet's shape to a spherical one accompanied by oscillations. Solution of hydrodynamic and electromagnetic equations, coupled with definition of the shape and position of the droplet was done within one software, ANSYS FLUENT, that allowed us to have a better coupling between multiphysic phenomena. It was found that use of Reynolds Stress Models for turbulent flow resulted in a good representation of oscillation of the droplet surface with the frequency close to theoretically predicted value. Estimation of a characteristic time for the decay of the oscillations is difficult and may be dependent on mesh size used in calculations that has to be studied further.

Acknowledgements The authors acknowledge financial support from the CNES under Material Sciences Program and from the ESA-MAP THERMOPROP, AO-1999-022.

A. Governing electromagnetic equations It is convenient to perform solution of the system of governing equations using complex presentation of harmonic fields with angular frequency $\omega = 2\pi f$. In this formalism, a real field $\mathbf{X}(\mathbf{r}, t)$ is given as

$$\mathbf{X}(\mathbf{r}, t) = \Re\{\hat{\mathbf{X}}(\mathbf{r})e^{i\omega t}\} \tag{11}$$

where $i^2 = -1$ is complex unit, $\hat{\mathbf{X}}(\mathbf{r}) = \hat{\mathbf{X}}_{Re}(\mathbf{r}) + i\hat{\mathbf{X}}_{Im}(\mathbf{r})$ is complex amplitude with real $\hat{\mathbf{X}}_{Re}(\mathbf{r})$ and imaginary $\hat{\mathbf{X}}_{Im}(\mathbf{r})$ part and $\Re$ is notation for taking the real part of complex number. In particular, this allows one to get rid of partial derivative on time:

$$\frac{\partial \hat{\mathbf{X}}(\mathbf{r})e^{-i\omega t}}{\partial t} = -i\omega t\hat{\mathbf{X}}(\mathbf{r})e^{-i\omega t} \tag{12}$$

Presentation of magnetic potential vector $\mathbf{A}$, density of the electric current $\mathbf{j}$ and electric potential V in their complex form similar to $\hat{\mathbf{X}}_{Re}(\mathbf{r})$ with further extraction of the real part of solution leads to system of equations written for their real and imaginary parts. Below it is given in a simplified form for cylindrical coordinate system (r, θ, z) which assumes that azimuthal θ-components of various field may exist, yet, no variation on θ is allowed, thus derivatives remain only on r and z coordinates.

$$\nabla\cdot\left(\sigma\nabla\hat{V}_{Re}\right)=\nabla\cdot\left(-\omega\sigma\hat{\mathbf{A}}_{Im}\right)$$

$$\nabla\cdot\left(\nabla\hat{A}_{r,Re}\right)=\mu_0\hat{j}_{r,Re}-\frac{\hat{A}_{r,Re}}{r^2}\quad\text{with}\quad\hat{j}_{r,Re}=\sigma\left(-\frac{\partial\hat{V}_{Re}}{\partial r}+\omega\hat{A}_{r,Im}\right)$$

$$\nabla\cdot\left(\nabla\hat{A}_{\theta,Re}\right)=\mu_0\hat{j}_{\theta,Re}-\frac{\hat{A}_{\theta,Re}}{r^2}\quad\text{with}\quad\hat{j}_{\theta,Re}=\sigma\omega\hat{A}_{\theta,Im}\quad(13)$$

$$\nabla\cdot\left(\nabla\hat{A}_{z,Re}\right)=\mu_0\hat{j}_{z,Re}\quad\text{with}\quad\hat{j}_{z,Re}=\sigma\left(-\frac{\partial\hat{V}_{Re}}{\partial z}+\omega\hat{A}_{z,Im}\right)$$

$$\nabla\cdot\left(\sigma\nabla\hat{V}_{Im}\right)=\nabla\cdot\left(-\omega\sigma\hat{\mathbf{A}}_{Re}\right)$$

$$\nabla\cdot\left(\nabla\hat{A}_{r,Im}\right)=\mu_0\hat{j}_{r,Im}-\frac{\hat{A}_{r,Im}}{r^2}\quad\text{with}\quad\hat{j}_{r,Im}=\sigma\left(-\frac{\partial\hat{V}_{Im}}{\partial r}-\omega\hat{A}_{r,Re}\right)$$

$$\nabla\cdot\left(\nabla\hat{A}_{\theta,Im}\right)=\mu_0\hat{j}_{\theta,Im}-\frac{\hat{A}_{\theta,Im}}{r^2}\quad\text{with}\quad\hat{j}_{\theta,Im}=-\sigma\omega\hat{A}_{\theta,Re}$$

$$\nabla\cdot\left(\nabla\hat{A}_{z,Im}\right)=\mu_0\hat{j}_{z,Im}\quad\text{with}\quad\hat{j}_{z,Im}=\sigma\left(-\frac{\partial\hat{V}_{Im}}{\partial z}+\omega\hat{A}_{z,Re}\right)$$

This system of equations is updated with conditions at external boundary of the calculation domain (Fig. 2) which are supposed to be at a large distance from the inductor that is equivalent to infinity. From numerical experiments it is found that results are not affected whether conditions for components of vector $\hat{\mathbf{A}}_{Re}=0,\hat{\mathbf{A}}_{Im}=0$ or "zero-flux" conditions $\partial\hat{\mathbf{A}}_{Re}/\partial n=0,\partial\hat{\mathbf{A}}_{Im}/\partial n=0$ are used in combination with similar conditions for electric potential, i.e. $\hat{V}_{Re}=0,\hat{V}_{Im}=0$ or $\partial\hat{V}_{Re}/\partial n=0,\partial\hat{V}_{Im}/\partial n=0$, $\partial/\partial n$ assumes derivative along normal vector to the boundary..

Relations of fields $\hat{\mathbf{A}}-\hat{V}$ with alimentation AC current is given through modified expression for the real part of the θ component of the electric current in eq.13:

$$\hat{j}_{\theta,Re}=\sigma\omega\hat{A}_{\theta,Im}+\hat{j}_{ext,i}\tag{14}$$

where $i=(p,d)$ is related either to positioning current of to the second current used to trigger the droplet oscillations. Once the problem for $\hat{\mathbf{A}}-\hat{V}$ is solved, the components of magnetic induction are found as

$$\begin{aligned}
&\hat{B}_{r,Re}=-\frac{\partial\hat{A}_{\theta,Re}}{\partial z} && \hat{B}_{r,Re}=-\frac{\partial\hat{A}_{\theta,Im}}{\partial z}\\
&\hat{B}_{\theta,Re}=\frac{\partial\hat{A}_{r,Re}}{\partial z}-\frac{\partial\hat{A}_{z,Re}}{\partial r}\equiv 0 && \hat{B}_{\theta,Im}=\frac{\partial\hat{A}_{r,Im}}{\partial z}-\frac{\partial\hat{A}_{z,Im}}{\partial r}\equiv 0\\
&\hat{B}_{z,Re}=\frac{\partial\hat{A}_{\theta,Re}}{\partial r}+\frac{\hat{A}_{\theta,Re}}{r} && \hat{B}_{r,Re}=\frac{\partial\hat{A}_{\theta,Im}}{\partial r}+\frac{\hat{A}_{\theta,Im}}{r}
\end{aligned}$$

Lorentz force averaged over period of oscillations is calculated according to the general expression that with complex variables gives

$$\bar{\mathbf{F}}=\hat{\mathbf{j}}_{Re}\times\hat{\mathbf{B}}_{Re}+\hat{\mathbf{j}}_{Im}\times\hat{\mathbf{B}}_{Im}\tag{15}$$

REFERENCES

1. G. Lohöfer and S. Schneider. Heat balance in levitation melting: Sample cooling by forced gas convection in Argon. *High Temperatures-High Pressures*, vol. 45 (2016), pp. 255–271.

2. R. Wunderlich and H. Fecht. Modulated electromagnetic induction calorimetry of reactive metallic liquids. *Measurement Sci. Techn.*, vol. 16 (2005), pp. 476–483.

3. M. Mohr, R.K. Wunderlich, K. Zweiacker, S. Prades-Rödel, R. Sauget, A. Blatter, R. Logé, A. Dommann, A. Neels, W. L. Johnson, and H.-J. Fecht. Surface tension and viscosity of liquid Pd43Cu27Ni10P20 measured in a levitation device under microgravity. *NPJ Microgravity*, vol. 5 (2019)

4. J. Etay, P. Schetelat, B. Bardet, J. Priede, V. Bojarevics, and K. Pericleous. Modelling of Electromagnetic Levitation – Consequences on Non-contact Physical Properties Measurements. *High Temp. Mater. Proc.*, vol. 27 (2008), pp. 127–132.

5. H. Lamb. *Hydrodynamics*, (Cambridge University Press 1975) pp. 127–132.

6. V. Bojarevics, and K. Pericleous. Modelling Electromagnetically Levitated Liquid Droplet Oscillations. *ISIJ International*, vol. 43 (2003), pp.890–898

7. S. R. Berry, R. W. Hyers, L. M. Racz, and B. Abedian. Surface Oscillations of an Electromagnetically Levitated Droplet. *Int. J. Thermophys.*, vol. 27 (2008), pp. 127–132.

8. S. Spitans, E. Baake, B. Nacke, and A.Jakovics. Numerical Modeling of Free Surface Dynamics of Melt in an Alternate Electromagnetic Field: Part II. Conventional Electromagnetic Levitation. *Met. Mat. Trans. B*, vol. 44B (2013) pp. 522–536

9. P. Chapelle, A. Jardy, D. Ablitzer, Yu. M. Pomarin, G. M. Grigorenko. High-speed imaging and CFD simulations of a deforming liquid metal droplet in an electromagnetic levitation experiment. *J. Mat. Sci*, vol. 43 (2008) pp. 3001–3008

10. A. Bansal, P. Chapelle, Y. Delannoy, E. Waz, P. Le Brun, and J.-P. Bellot. Experimental and numerical analysis of the deformation of a liquid aluminum free surface covered by an oxide layer during induction melting. *Met. Mat. Trans. B*, vol. 46 (2015), pp.2096–2109

11. ANSYS FLUENT user's guide ANSYS Inc., ver. 16.2.0 edition, 2016.